Fuel 302 (2021) 121160

Contents lists available at ScienceDirect

Fuel

journal homepage: www.elsevier.com/locate/fuel

Combustion characteristics of a single droplet of hydroprocessed vegetable oil blended with aluminum nanoparticles in a drop tube furnace

Inês A. S. Ferrão [a,b,c], André R.R. Silva [a,*], Ana. S.O.H. Moita [b,d], Miguel A.A. Mendes [c], Mário M. G. Costa [c]

[a] AEROG, Universidade da Beira Interior, Covilhã, Portugal
[b] IN+, Instituto Superior Técnico, Universidade de Lisboa, Lisboa, Portugal
[c] IDMEC, Instituto Superior Técnico, Universidade de Lisboa, Lisboa, Portugal
[d] CINAMIL, Portuguese Military Academy, Lisboa, Portugal

ARTICLE INFO

Keyword:
Single droplet combustion
Free - falling droplet experiment
Aviation alternative fuel
Micro-explosions

ABSTRACT

This study examines the burning characteristics and disruptive burning phenomena of single droplets of aluminum nanoparticles (n-Al) stably suspended in a biofuel (HVO). The biofuel used in the present work is a promising alternative fuel already tested in the aviation sector to reduce greenhouse gas and pollutant emissions. Experiments were conducted with two particle sizes (40 nm and 70 nm) and two particle concentrations (0.5 wt. % and 1.0 wt.%) to study its influence when added to the biofuel. The effect of size and concentration of the aluminum nanoparticles was studied at 1100 °C in a drop tube furnace. This experimental facility allows the study of combustion characteristics of falling droplets, ensuring there is no influence of the supporting fiber on the burning rate and disruptive burning phenomena occurrence. A CMOS high - speed camera coupled with a high magnification lens was used to evaluate the droplet size, burning rate, and micro-explosions. Based on this procedure, pure biofuel droplets were compared with those of biofuel blended with nanoparticles. The results suggest that the combustion characteristics of pure HVO can be enhanced with the addition of aluminum nanoparticles. Furthermore, by decreasing the particle size, a slight increase in the burning rate of nanofuels was noticed. Additionally, an increase in the particle concentration leads to a pronounced increase in the burning rate. The particle concentration also influences the delay and intensity of micro-explosions, disruptive burning phenomena detected at the end of the droplet lifetime.

1. Introduction

Aviation contributes with approximately 2% of the global CO_2 emissions and its activity grew around 140% between 2000 and 2019. Additionally, an annual growth rate of 3.5% for the passenger numbers is expected for the next two decades [25,35]. The aeronautical sector is the second largest sector in transportation and operates with a single multicomponent fuel, namely jet - fuel, which is sourced from fossil fuel. There are two commercial jet - fuels, Jet A-1 in EU and Jet A in USA. Jet fuel is primarily constituted by a mixture of alkanes, olefins, aromatics, and small quantities of non–hydrocarbon molecules, including e.g. sulfur atoms [59]. High energy content, well-defined flow characteristics, and thermal stability are several requirements of this fuel to be appropriately used in aero-engines [8]. The significant growth of this sector allied with environmental concerns and depletion of fossil fuels has promoted the investigation on the use of potential alternative fuels in aviation gas turbines due to their renewability, potentially lower emissions, and energy security.

Alternative fuels are a renewable energy source derived from sustainable feedstock considered as potential carbon neutral fuel which reduces pollutant emissions. Specifically, biofuels can be sourced from firewood, animal fats and oils, animal dungs, and vegetable oils. The use of alternative fuels reduces the risk of scarcity with the variability of energy sources and reduces oil dependence, being a finite natural source [44]. Table 1 shows the different categories and technology pathways of alternative fuels. As noted earlier, taking into consideration safety and airworthiness, five biofuel fuel production technologies were approved for the aviation sector (ATJ-SPK, SIP-SPK, FT-SPK, FT-SPK/A and HEFA) [13,42].

In terms of readiness, HEFA could be a solution for the immediate,

* Corresponding author.
E-mail address: andre@ubi.pt (A.R.R. Silva).

https://doi.org/10.1016/j.fuel.2021.121160
Received 17 February 2021; Received in revised form 10 May 2021; Accepted 28 May 2021
Available online 17 June 2021

Table 1
Summary of biofuel production technologies. Adapted from [13,42].

Category	Technology Pathway	Feedstock	Process Description
Alcohol to Jet	ATJ-SPK (Alcohol to Jet Synthetic Paraffinic Kerosene)	Cellulosic, biomass, starch, sugar	Hydrolysis of biomass → Sugar fermentation to alcohol → Dehydration → Oligomerization → Hydrogenation → Fractionation
Gas to Jet	FT-SPK (Fisher-Tropsch-Synthetic Paraffinic Kerosene)	Coal, biomass, natural gas	Gasification of biomass → Fischer–Tropsch → Hydroprocessing
	FT-SPK/A (Fisher-Tropsch-Synthetic Paraffinic Kerosene with Aromatics)	Coal, biomass, natural gas	Gasification of biomass → Fischer–Tropsch → Hydroprocessing → Increase aromatic content
Oil to Jet	HEFA (Hydroprocessed Esters and Fatty Acids)	Algal oil, animal fat, recycled oil, vegetable oil	Deoxygenation of oils and fats → Hydroprocessing
Sugar to Jet	SIP-SPK (Synthetic Isso-Paraffinic)	Any fermentable sugar	Hydrolysis of biomass → Sugar fermentation to farnesene → Hydroprocessing → Fractionation

cost-effective implementation in the aviation sector, where the fuel quality is independent of the feedstock used. On the other hand, the lack of aromatics could lead to sealing issues in existing engines. The FT and ATJ produce synthetic jet - fuel content to be used, avoiding fuel seal concerns.

HEFA commercial production still presents concerns regarding feedstock availability and production complexity [13]. Hydroprocessed vegetable oil (HVO) is obtained from HEFA which offers a high energy density when compared to other biofuels and promotes a significant reduction in greenhouse gas and pollutant emissions. HVO presents good cold flow properties, high cetane number, high thermal stability, and is free of aromatic and sulfur content [20,23]. Studies focusing on comparing jet-fuel and biofuel produced from HEFA have been developed for single droplet combustion and tested in gas turbine engines [10,33,38]. In general, satisfactory results are obtained, showing significant improvements in pollutant emissions. However, understandings of fundamentals of HVO combustion characteristics are necessary, such as flame speed, extinction, reactive species quantification effects on combustion performance, to understand and compare the biofuel combustion efficiency for specific conditions [4,9].

A challenge to implement these alternative fuels in the aeronautical sector is the restricted fuel requirements that should comply with the current legislation. Moreover, a novel liquid fuel must be interchangeable with the current jet - fuel to promote reliable and proper aeronautical activity management. Subsequently, the research focus is on the development of a “drop-in” fuel, the main reason being the industry keeping its assets in use for several years due to the high investment cost [8]. Thus, a significant evaluation of the use and production of alternative aviation fuels has been made in the last 20 years. The first airline to perform a flight using kerosene and biofuel was Virgin Airlines in February 2008. The viability and safety of using biofuel were tested and from that point, numerous flights used blends of biofuel and jet - fuel in different volume percentages [6,8,42]. However, biofuels present important drawbacks related to low energy content, high viscosity, lower volatility properties and high production costs. In particular,

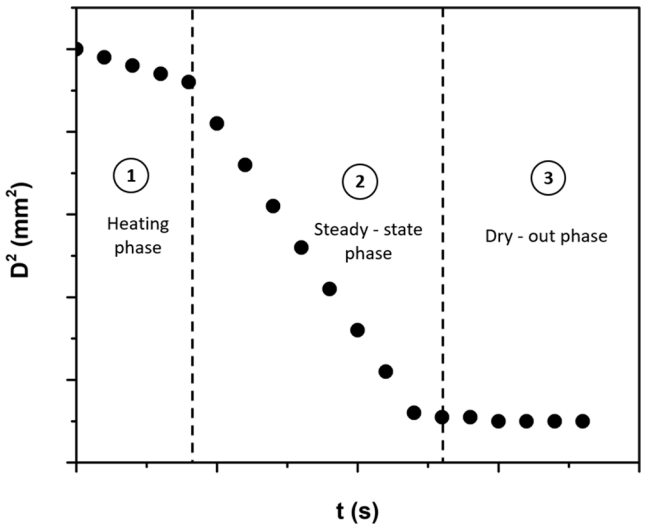

Fig. 1. Illustration of the droplet size evolution for nanofuel droplet evaporation adapted from [18,29].

biodiesel and alcohols possess reduced energy content compared with jet fuel, leading to an increase in fuel volume usage and a decrease in fleet-wide energy efficiency [24]. Moreover, a reduction in production costs relies on feedstock availability, which is not being produced commercially [24,34,44].

To enhance the performance of biofuels, a possible approach is the addition of nanoparticles. Nanoscale energetic metal particles add to fuel could enhance the combustion performance in terms of: increase of volumetric energy density, enhancement of the catalytic activity, low ignition delay, higher ignition probability, higher volumetric heat release rates, faster burning rates, among others. The so-called nanofuels combine the high specific surface area of nanoparticles and the high oxidation energy of metals to produce high energy density fuels, improving the fuel economy and reducing pollutant emissions [1,5].

The use of energetic metal particles in propellant rockets and explosives has shown advantages in terms of ignition and combustion performance. Aluminum particles have been an additive for these systems due to their relatively low cost and high combustion enthalpy [30]. In the last decades, studies were mostly based on micron-size particles, however, through research and development of nanotechnology, a novel class of fuels arose. Nanoparticles in a range of 1–100 nm, compared with micron-size particles present a higher specific surface area, higher reactivity, stability and the potential to store energy at the surface [19]. Energetic metal nanoparticles present a high energy density, mainly due to their higher gravimetric and volumetric heating values when compared to hydrocarbon fuels, as reported by [56]. Consequently, researchers have been focused on understanding how the addition of the nanoparticles can improve the thermophysical properties of the fuel.

An early study developed by [52] addressed the addition of small quantities of n-Al (aluminum nanoparticles) and n $-Al_2O_3$ (aluminum oxide nanoparticles) to a liquid fuel. The authors reported that the ignition probability for diesel with nanoparticles is considerably higher than for pure diesel. This new class of fuels has already shown an enhancement of the evaporation rate compared to the pure fuel. [50] studied the effect of droplet size on the combustion behavior of pure ethanol and ethanol with aluminum nanoparticles. The authors reported that the burning rate rises with increasing particle concentration. It was also found that the absorption of radiation energy emitted is a relevant mechanism to enhance the burning rate of nanofuels. [28,29] evaluated experimentally the evaporation behavior of kerosene droplets blended with dilute and dense concentrations of aluminum nanoparticles, at elevated temperatures. It was concluded that the nanofuel droplet lifetime were shorter than pure kerosene droplets at high temperatures.

However, the authors also reported that for higher particle concentration, more concretely above 2.5 wt%, burning rate decreases. Additionally, [21] report that the addition of nanoparticles may imply a decrease in the burning rate. The contradictory findings related to the evaporation rate, which are reported in the literature, may be a consequence of different methods and experimental conditions considered in various evaporation studies [46]. According to [50,51], the droplet size is an important feature, which clearly influences the aggregation timescale. Hence, when small droplets (of the order of 200 microns) are used, the nanoparticles existing inside the droplet may not have sufficient time to completely aggregate until the end of the droplet lifetime due to its small size and consequent very short lifetime. The burnt aggregates were evaluated, and it was noticed that their size was an order of magnitude smaller than that of the primary droplet. These studies identified three phases during the nanofuel droplet evaporation mechanism: (1) heat - up, (2) steady - state, and (3) dry - out. Fig. 1 shows an illustration of the nanofuel droplet evaporation.

The dry - out phase corresponds to the last stage of the nanofuel droplet lifetime, where residual nanoparticles can be detected at the end of the steady - state phase or disruptive burning events [14]. [18] observed these three phases to study the evaporation characteristics of fuel droplets with the addition of nanoparticles under natural and forced convection. The authors stated that at a relatively low temperature under forced or natural convection, the evaporation rate for nanofuels does not follow the classical D^2-law. However, a different behavior was noticed for higher temperatures under forced convection. [17] also investigated the burning characteristics of a single nanofuel droplet suspended, using nano - and micro - sized aluminum particles added to ethanol and n-decane. They reported that, for the same surfactant concentration, the micro - explosion behavior of suspensions using micron particles occurred later than for suspensions with nanoparticles and with much stronger intensity. Several authors [17,21,28] found a disruptive burning phenomenon, namely micro-explosions that occur when the primary droplet disintegrates into smaller droplets, enhancing the combustion process. According to [28], increasing the ambient temperature and particle concentration promotes the appearance of these phenomena earlier in the droplet lifetime. At 700 ºC and 800 ºC, the micro-explosions significantly enhance the evaporation rate.

The micro-explosion phenomenon was already reported in several studies involving emulsions. According to [2], the origin of this phenomenon is the different volatility in fuels. The difference in the fuel boiling point leads to the nucleation of gas bubbles of the most volatile component. The nucleation process appears when the superheat limit of the emulsion surpasses the boiling point of the fuel droplet, [3,27]. The occurrence of micro-explosions enhance the effective fuel droplet size distribution, air–fuel mixing, and ultimately fuel efficiency [45].

More recently, [54] performed a numerical study on the evaporation rate of a copper–water nanofluid droplet. The authors reported that the D^h - law is influenced by the nanoparticles used in the study. For a pure liquid, the exponent h is about 2. However, this exponent will be less than 2 for lyophilic nanoparticles (i.e. attracting the liquid), and greater than 2 when lyophobic nanoparticles (i.e. repelling the liquid) are added. These results also confirm the decrease of the average evaporation rate of the nanofluid droplet at the end of droplet evaporation due to the aggregation of the nanoparticles on the surface, resulting in a shell. According to several authors, [7,37], when the liquid fuel is gradually consumed, the average evaporation rate decreases significantly due to the formation of a surface shell. This shell is generated due to the increase of nanoparticle concentration at the droplet surface and is characterized by a constant droplet diameter until the appearance of a micro-explosion. Consequently, the fuel spreading from the core towards the droplet surface is blocked by this shell, thus reducing the evaporation rate [37]. The internal pressure inside the droplet increases due to the liquid fuel vaporization that remains inside the droplet, allowing the break of the surface shell layer and leading to a micro-explosion. [7] evaluated the burning process of multiple liquid fuels with various nanoenergetic additives in the suspended droplet configuration. [7] noticed that ethanol with 5 wt.% soluble ammonia borane and RP-2 with 1 wt.% presented the most promising results to be further investigated in a reactive liquid nanofuel spray.

Table 2
HVO and Jet A-1 fuel properties adapted from [12,40,43].

Parameter	HVO	Jet A-1
Density (kg/m^3) (at 20 °C)	780.6	798
Surface tension (N/m) (at 20 °C)	0.0265	0.0247
Kinematic viscosity (mm^2/s) (at 25 °C)	4.33	1.40
Sulfur (wt.%)	0.09	0.3
Aromatics (wt.%)	0	13.8
Flash point (°C)	99	38
Final boiling point (°C)	308	237
Cloud point (°C)	−30	−26
Lower heating value (MJ/kg)	43.9	43
Higher heating value (MJ/kg)	47.1	47
Distillation 10 vol.% (°C)	262	170
Hydrogen content	15.4	14.5
Carbon content	85.5	84.6
H/C ratio	2.18	1.91
Average chemical composition	$C_{15}H_{32}-C_{18}H_{38}$	$C_{11}H_{21}$

Table 3
Bulk properties of aluminum [16].

Parameter	Value
Density (kg/m^3)	2700
Melting point (°C)	660
Boiling point (°C)	2519
Heat of combustion (MJ/kg)	31.1

The literature reviewed in the previous paragraphs evidences a relatively sparse number of studies focusing on the use of nanoparticles in alternative fuels for aviation. In this sector, biofuels have been a relevant topic in order to mitigate the problems regarding greenhouse gas and pollutant emissions. However, these alternative fuels present a reduced performance when compared to jet fuel. Due to this, the present work studies the addition of nanoparticles in a biofuel. This experimental study compares the burning characteristics of pure HVO and HVO with aluminum nanoparticles, aiming to describe the effect of nanoparticle size and concentration on evaporation and combustion of the fuel droplets. To accomplish it, falling droplets burning at elevated temperature in a drop tube furnace was evaluated. This investigation allows the visualization of the droplet movement and combustion without using a supporting fiber, which could influence disruptive burning phenomena as a vapor bubble nucleating agent and other significant burning characteristics in this kind of study. Additionally, the disruptive burning phenomena of nanofuels will also be addressed.

2. Materials and methods

2.1. Nanofuel preparation and characterization

The base fuel used in this work was an hydroprocessed vegetable oil (HVO) named NExBTL. As noted earlier, this alternative fuel, commonly referred to as renewable diesel obtained from HEFA, is typically made from vegetable oils [15,45]. Table 2 shows the properties of the HVO from NESTE and Jet A-1, a conventional jet-fuel.

Four nanofuels composed of HVO and aluminum nanoparticles were used in this work. Pure HVO was also tested for comparison purposes. Aluminum is a suitable additive to hydrocarbons due to its abundance, amount of energy release, and relatively low production cost [22]. Table 3 shows the bulk properties of aluminum, produced by Nanografi, as those used by [16]. Two particle sizes (40 nm and 70 nm) and two

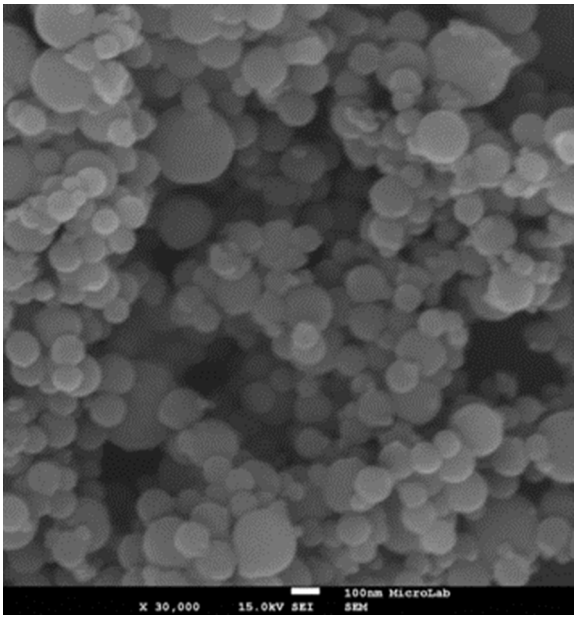

Fig. 2. SEM images of aluminum nanoparticles (40 nm).

Table 4
Nanofuels physical properties.

	Aluminum nanoparticles (n-Al)		Density (kg/m^3)	Surface tension (N/m)	Viscosity (Pa.s)
	Size (nm)	Concentration (wt.%)			
HVO	40	0.5	771.4	0.0265	0.020
	70	0.5	771.6	0.0265	0.025
	40	1.0	773.2	0.0267	0.055
	70	1.0	778.5	0.0267	0.050

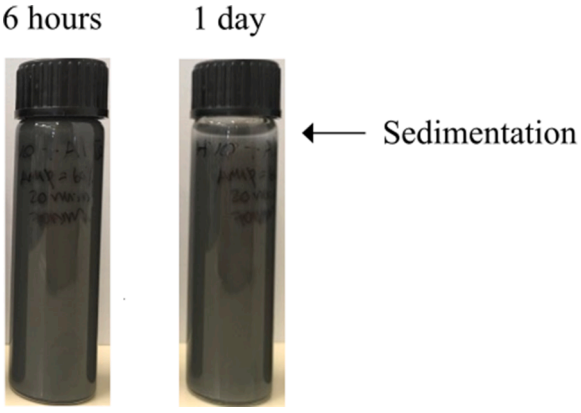

Fig. 3. Evolution of nanofuel stability for HVO + 70 nm (1.0 wt.%).

particle concentrations (0.5 wt.% and 1.0 wt.%) were used. The aluminum nanoparticles with a size of 40 nm, used in the present study, is displayed in Fig. 2. Table 4 shows the nanofuels used in the present study and their physical properties. The density was measured with the pycnometer method, and the surface tension was measured at room temperature (20 ± 3 ºC) with an optical tensiometer THETA (Attension). To determine the surface tension, the pendant drop method was used. A detailed description of the measurement procedures can be found in [39]. The viscosity was determined using a rheometer (TA instruments ARI 500 ex), at ambient temperature, with an accuracy of ±5%.

The suspension stability is a crucial aspect in nanofuel studies. The nanofuels preparation demands a methodic procedure to accomplish homogeneous, stable, long - term suspensions and a low - level particle agglomeration [17]. In this study, the nanoparticles were first vigorously stirred for 20 min with the liquid fuel, using a magnetic stirrer. Subsequently, the nanofuels HVO + n-Al were sonicated in an ice bath. The sonicator (model UP200Ht by Hielscher) was used to disperse the particles and to avoid agglomeration, with an amplitude of 20% for a period of 30 min for each nanofuel. Afterward, the nanofuels stability was evaluated for several hours and days in a test tube by visual inspection. The observations revealed that the nanofuels with a particle concentration of 0.5 wt.% are more stable than the nanofuels with a particle concentration of 1.0 wt.%. The nanofuel HVO + n-Al with a particle concentration of 0.5 wt.%, does not show evident sedimentation for a time interval of 24 h. The HVO + n-Al with a particle concentration of 1.0 wt.% lasted almost 6 h as a homogeneous solution with no evident sedimentation, as shown in Fig. 3. A particle concentration of 3.0 wt.% was also tested. However, the nanofuel HVO + n-Al (3.0 wt.%), for both particle sizes, was only stable for a short period, approximately 20 min, thus it was not possible to obtain accurate results. Due to this, the single droplet combustion was only investigated for two particle concentrations and two particle sizes, as already mentioned. A forthcoming study is to add surfactants to the nanofuels with the purpose of increasing the stability of these fuels.

2.2. Experimental setup and procedures

Fig. 4 shows a schematic of the experimental setup. It consists of an electrically heated drop tube furnace (DTF), an illumination set, an image acquisition system, and an injector device. The single droplet combustion occurs inside a vertical quartz tube with an inner diameter of 6.6 cm and a length of 82.6 cm. A more detailed description can be found in a previous study [41]. The DTF has two opposed rectangular windows with 2 cm width and 20 cm height.

The illumination set, which comprises an LED light and a diffusion glass, was placed in front of one of the rectangular windows. This illumination system enhances the contrast and thereby, the visualization of the droplet evaporation/burning process. The image acquisition system was placed in front of the other rectangular window. This system is composed of a CMOS high - speed camera (CR600 × 2, Optronics), placed perpendicularly to the quartz tube and a computer, being the camera manually triggered. The CMOS camera only provides images with a grayscale defined by the intensity of the luminosity captured. The camera was attached to a high magnification lens (Zoom 6000® Lens System). The magnification lens is composed of a 6.5 × Zoom, 12 mm FF, a 0.25× lens attachment, and a 2.0× short adapter, with a magnifying range of 0.35–2.25. The image acquisition was pursued with 1000 fps with a resolution of 1280 × 500 pixels and an exposure time of 1/12000 s.

Regarding the air supply, a flow rate of 5.7 L/min with a precision error of ± 2% was used. When the air enters, the quartz tube is heated and generates a proper environment to occur the droplet autoignition. It is important to highlight that the air enters the quartz tube prior to the droplet injection from a different inlet, as shown in Fig. 4.

The injection equipment is a TSI device with a pinhole diameter of 200 µm, which generates monosized droplets. The droplet generator was placed on top of the DTF and connected to a syringe pump and a frequency generator. To release the droplets, a syringe with a volume of 50 mL is coupled to the syringe pump, feeding the fuel to the droplet generator. The stream of droplets with an initial diameter of 250 ± 8 µm was achieved for the operating conditions of 2.1 kHz and a flow rate of 1.3 mL/min.

During the experiments, no evident particle sedimentation was detected in the injection system. The droplet stream produced by the monosize droplet generator does not guarantee the space/time between

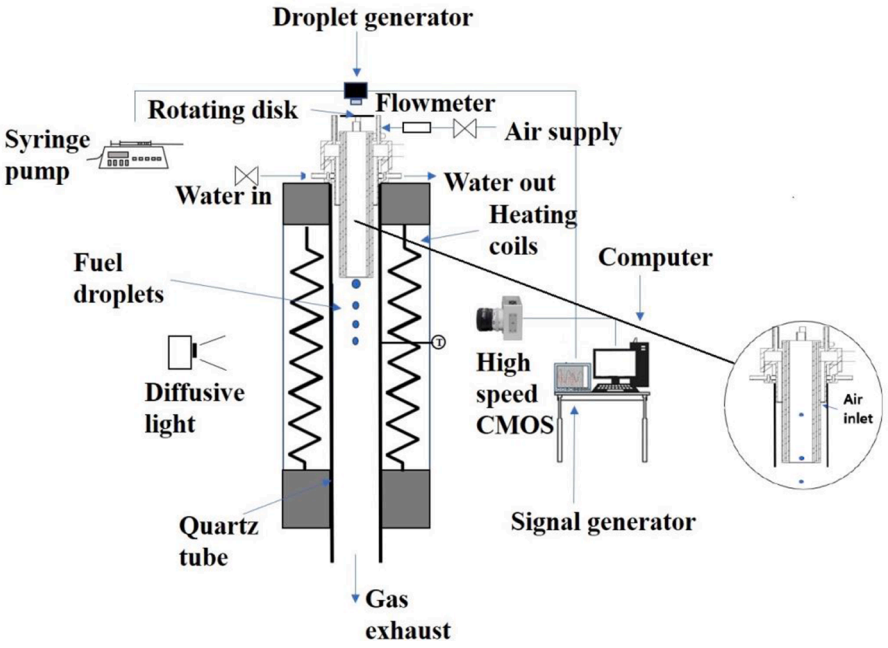

Fig. 4. Schematic of the experimental setup [41].

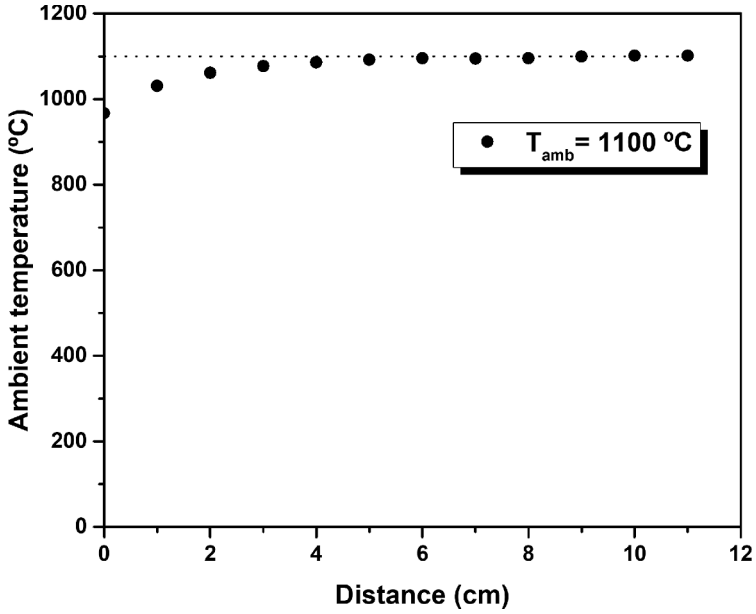

Fig. 5. Temperature profile along the quartz tube.

droplets to ensure a single droplet phenomenon; hence, a rotating disk with a slot was used to increase the inter-droplet distance. The slot dimensions are 1 cm x 1 cm, and the disk diameter is 12 cm with a rotational speed of 1200 rpm. According to the literature, to guarantee the phenomena of single droplet combustion, a minimum droplet spacing of 30 droplet diameters is required, as reported by [11]. In this way, it is ensured a droplet spacing larger than 50 droplet diameters in the present work. Hence it is guaranteed that there is no droplets interaction. This experimental setup allows studying the combustion of micrometric nanofuel droplets at T = 1100 ºC and atmospheric pressure, without using supporting fiber avoiding its influence on the dynamic behavior of the droplet [53].

Fig. 5 shows the temperature profile along the quartz tube at the test temperature (T = 1100 ºC). The injector tip is represented by x = 0 cm. The temperature profile was measured with a fine wire thermocouple type R with a size of 76 μm.

An image detection algorithm was used in order to detect the droplet and determine its properties (e.g, droplet diameter, droplet velocity, among others). The data were treated in the ImageJ software. The edge detection and the pixel values were acquired through the Huang threshold method. A ROI (region of interest) of the entirety of the droplet was defined, calibrating the thresholds of the methods for an accurate measurement of the droplet. The transition from light to darker gray near the surface of the droplet is characterized by a pronounced brightness gradient, representing the droplet outline. To determine the droplet outline, the brightness difference between the lighter background, the darker droplet and the local gradient of brightness were considered. The brightness gradient was calculated for each pixel in

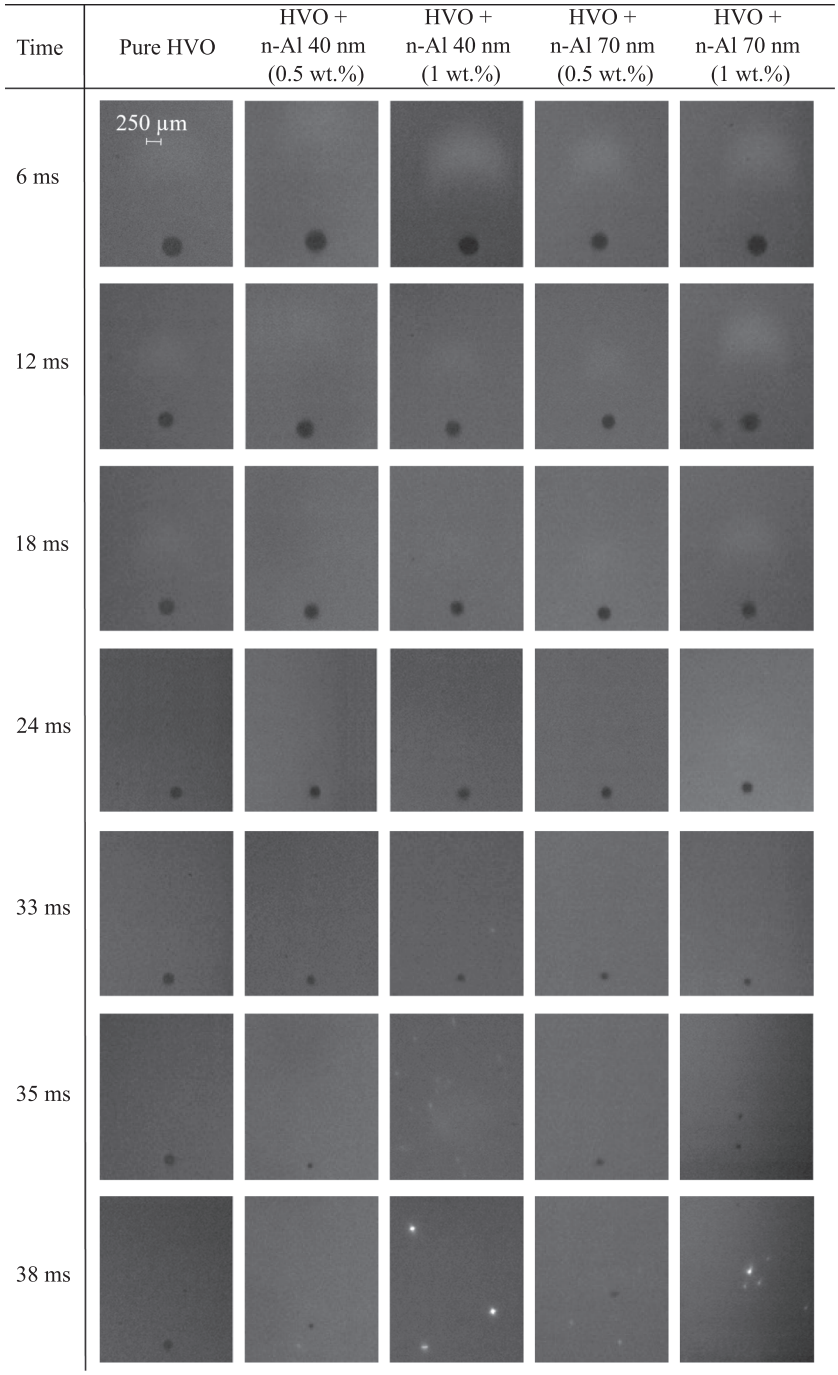

Fig. 6. Sequences of instantaneous images of burning droplets at 1100 °C of the pure HVO and the four nanofuels (D_0 = 250 µm, atmospheric pressure).

each image containing a droplet. There was a sharp transition from light gray to darker gray pixels near the fuel droplet surface. Subsequently, the droplet diameter was determined through the instantaneous droplet area given by image analysis related to a circle $A = \pi r^2$, where r is the droplet radius. For the optical configuration used in this work, the pixel size was 12 µm.

As already mentioned, the initial droplet diameter is D_0 = 250 µm and to evaluate the convective effects, the Reynolds, Prandtl and Nusselt numbers were determined by the following equations [26]:

$$Re = \frac{\rho|U_d - U|D_0}{\mu} \tag{1}$$

$$Pr = \frac{\mu C_p}{K} \tag{2}$$

$$Nu = 2 + \frac{0.555 Re^{1/2} Pr^{1/3}}{\left[1 + \frac{1.232}{RePr^{4/3}}\right]^{1/2}} \tag{3}$$

Where ρ is the density and μ is the viscosity considering an ambient temperature of 1100 °C. The specific heat C_p and the thermal conductivity K were determined from [58] and $|U_d - U|$ corresponds to the relative droplet velocity achieved through the droplet velocity and the flow velocity. To measure the droplet velocity, the droplet centroid was determined from sequential frames and consequently divided by the time of two frames. Thus, for these experimental conditions, the

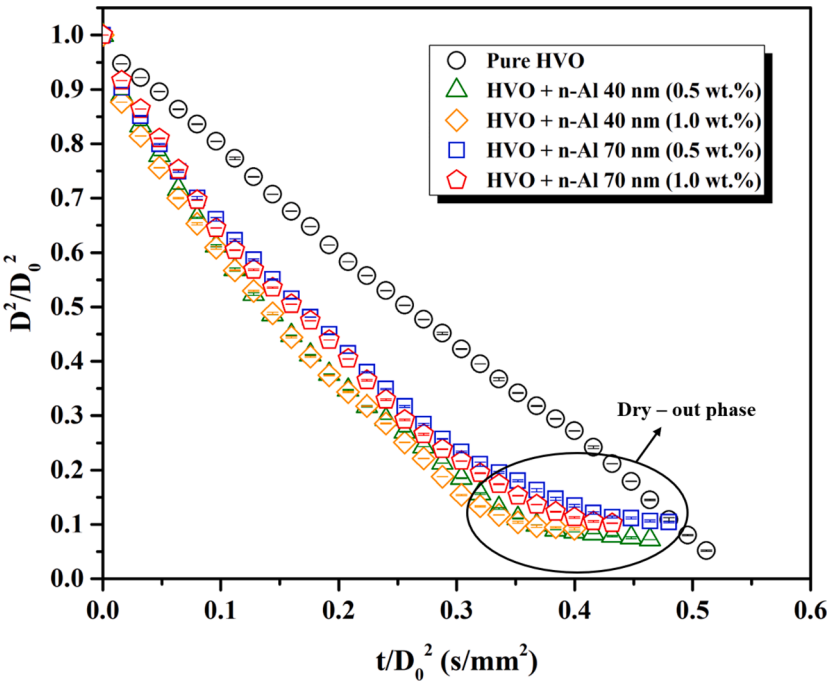

Fig. 7. Square of the normalized droplet diameter as a function of the normalized time at 1100 ºC for the pure HVO and the four nanofuels (D_0 = 250 μm, atmospheric pressure).

maximum droplet Reynolds number was approximately 0.8, and for a Prandtl number of 0.7, the maximum Nusselt number was 2.2. These values are determined taking into consideration the initial droplet diameter. Hence, as time evolves, the droplet diameter reduces, leading to a decrease in the Reynolds and Nusselt numbers. Due to this, we can affirm that the convective effects will be diminished with the droplet size reduction. As mentioned previously, for the experimental conditions, the maximum droplet Reynolds number is 0.8. According to [26] if Re ⩽2, the separation effects are negligible. Thus, the experimental work occurs under forced convection in a laminar regime (stationary).

A statistical study was performed to evaluate the number of droplets that should be used to assure that the droplet size evolution curve and burning rate were independent of the size of the sample. Therefore, the droplet size evolution and burning rate were evaluated as a function of the number of droplets, using 10 to 45 droplets for each nanofuel. In the present work, a minimum of 35 droplets is needed in order to have a statistical convergence, where no significant variation in the droplet size evolution curves and burning rate were noticed. Subsequently, the D^2/D_0^2 curves will be presented considering 40 droplets with a standard deviation of 0.05, as will be described later.

3. Results and discussion

3.1. Description of combustion behavior of single droplets

In this section, the combustion of pure HVO and HVO + n-Al single droplet will be qualitatively and quantitative compared in terms of micro-explosion occurrence, droplet size regression, and droplet flame. Fig. 6 shows sequential images of a droplet of pure HVO and HVO with different sizes and concentrations of aluminum nanoparticles burning at 1100 ºC. It is essential to mention that the different instants (t) correspond to a droplet burning in different vertical positions at the drop tube furnace, followed by the CMOS high-speed camera. For these experiments, five different camera positions were used to guarantee the visualization and analysis in detail of the droplet lifetime.

Prior to the droplet injection, the air inside is heated by the electric coils at the DTF and creates an appropriate environment to evaluate the pure HVO and HVO + n- Al combustion. When the droplet enters the quartz tube, it heats and ignites, which consequently leads to the formation of a diffusion flame. The frame when the ignition is detected, characterized by the appearance of a diffusion flame, is defined as t = 0 ms. The droplet diameter measurements have begun approximately 1 cm from injector tip when ignition occurs. To occur the autoignition, the droplet is exposed to a high ambient temperature. Subsequently, vaporization arises from the droplet surface generating a proper proportion of fuel/air mixing leading to the droplet autoignition. The flame is established at the droplet wake for all fuels, and flame intensity decreases as the droplet shrinks along its lifetime. The flame intensity of the pure HVO is apparently less intense than the HVO with aluminum nanoparticles. However, the flame intensity is difficult to compare in terms of visualization, indicating that further studies regarding this subject should be performed to verify the trend for nanofuels. Besides the flame intensity, the addition of nanoparticles is also noticed in the reduction of droplet diameter. Fig. 6 shows different instants of the single droplet combustion to evaluate the reduction of droplet size, where the pure HVO displays a longer lifetime. The nanofuel HVO + n-Al 40 nm (1.0 wt.%) depicts the fastest regression of droplet diameter. A mechanism responsible for reducing the droplet lifetime in nanofuels is micro-explosions, which occurs in the final phase: dry - out. When the droplet reaches a critical size, a disruptive burning phenomenon, namely micro-explosion occurs [21,28].

The pure HVO provides a steady burning until reaching the end of the droplet lifetime, while all the nanofuels in use exhibit micro-explosions at the end of their lifetime, regardless of the particle size and concentration. The detection of this event occurs when agglomerates of nanoparticles leave the primary droplet and ignite, producing intense bright spots. For a lower concentration HVO + n-Al 40 nm (0.5 wt.%), micro-explosions occurred at later time instants. As shown in Fig. 6, the micro-explosion of HVO + n-Al 40 nm (1.0 wt.%) occurs at t = 33 ms, and the micro-explosion of HVO + n-Al 40 nm (0.5 wt.%) at t = 38 ms, approximately 5 ms later. The onset of micro-explosions shows that an increase in the particle concentration and reduction in the particle size promote the occurrence of micro explosions earlier in the droplet lifetime, even though these phenomena only occur with a slight

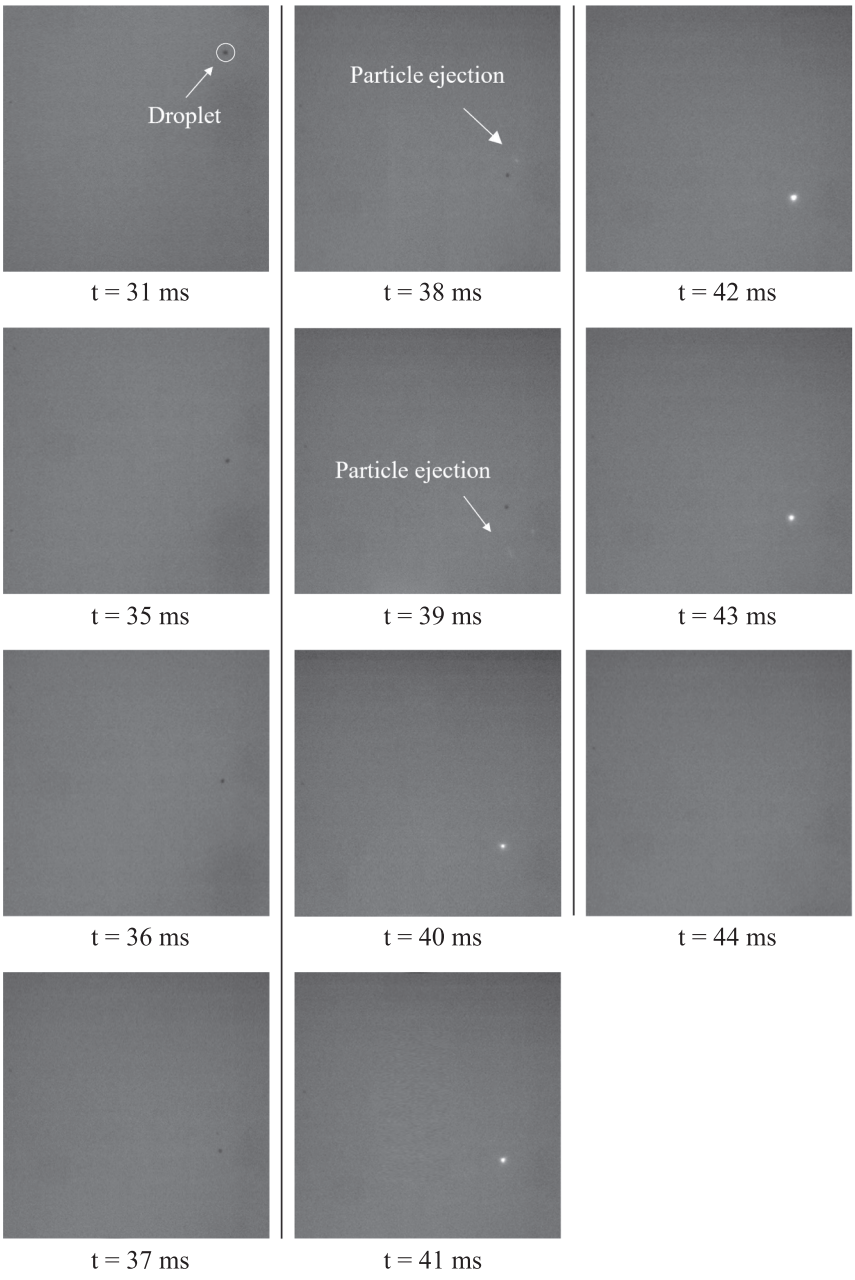

Fig. 8. Sequence of instantaneous images of the micro-explosion of an HVO + n-Al 40 nm (0.5 wt.%) (D_0 = 250 μm, T = 1100 °C, atmospheric pressure).

instant difference. In order to follow the visualization of droplet diameter reduction between all fuels as shown in the previous images, Fig. 7 shows the square of the normalized droplet diameter (D^2/D_0^2) as a function of the normalized time (t/D_0^2). For the representation of each D^2 curve, 40 droplets were used. To smoothen the curves, a five-point moving average was employed in D^2 curves.

The initial droplet diameter (D_0) corresponds to the droplet diameter as it enters the quartz tube and ignites. As observed in Fig. 6, the droplet size evolution of the pure HVO and the nanofuels are quite different, mainly at the end of the droplet lifetime. For nanofuels, the last phase of the droplet lifetime is named dry - out phase, which begins approximately at $t/D_0^2 = 0.38$ (s/mm^2) and is represented by a black circle in Fig. 7. The nanoparticle dynamics inside the droplet affect the droplet evaporation. Comparing the nanofuels, the D^2 curves practically overlap, where a slight difference can be detected from each particle size.

As already observed, the transition from the steady - state to the dry - out phase is related to the particle concentration. It indicates no great difference between the droplet size evolution curves in this range of particle size (40 nm and 70 nm). However, the present results are in agreement with the literature findings, i.e., a reduction in the particle size leads to an increase the wet surface area when a constant particle concentration is considered. This fact promotes an increase in the evaporation rate.

For pure HVO, it can be affirmed that the droplet follows the classical liquid droplet combustion theory, however, for nanofuels, the curves present a different behavior indicating that the presence of nanoparticles influences the droplet size evolution. Additionally, the particle size and concentration affect the curves, these relevant details have a notorious influence at the dry - out phase, where micro-explosions are spotted. The following sections are dedicated to understanding these disruptive burning phenomena and a more detailed description regarding the droplet size evolution for a pure HVO and HVO + n-Al. It is essential to mention that the ambient temperature greatly affects the

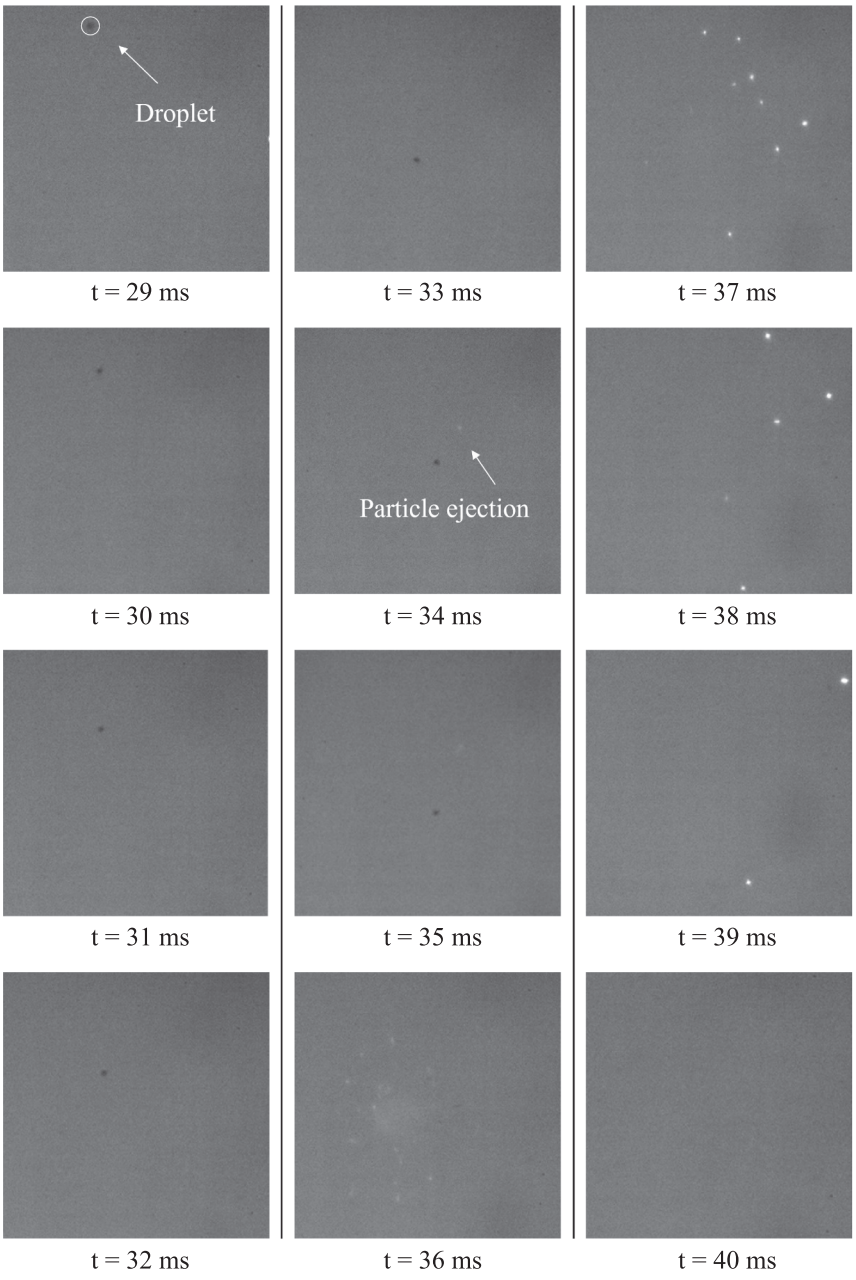

Fig. 9. Sequence of instantaneous images of the micro-explosion of an HVO + n-Al 40 nm (1.0 wt.%) (D_0 = 250 μm, T = 1100 ºC, atmospheric pressure).

droplet combustion behavior. The ambient temperature of the present work is considerably higher than the boiling point of the fuel and the melting of aluminum. An ambient temperature of T = 1100 ºC was tested, which leads to fast initial heating of droplet and considerable radiative heat transfer.

3.2. Disruptive burning phenomena

Fig. 8 shows a sequence of images of the micro-explosion of HVO + n-Al 40 nm (0.5 wt.%). This sequence of images corresponds to the end of the droplet lifetime that demonstrates in detail and sequentially this phenomenon for a droplet of HVO + n-Al 40 nm (0.5 wt.%). The visualization of this phenomenon permits to understand and describe how it influences droplet combustion. Based on this, when the liquid fuel is mostly consumed, the droplet presents a different behavior, where a considerable amount of nanoparticles remains inside the droplet. This behavior means that, as the biofuel is evaporating, the aluminum nanoparticles are concentrating at the droplet surface. The agglomeration of nanoparticles hinders the vaporization of the liquid fuel and promotes local hot spots. The presence of a hot spot increases the local droplet temperature and induces biofuel vapor nucleation, leading to a micro-explosion [36]. According to [49,55], to analyze the relative motion of the regressing surface and particles, the Peclet number (Pe) should be studied. The final particle morphology after the liquid evaporate could be given by this dimensionless number.

$$Pe \equiv \frac{K}{8D} \tag{4}$$

Where K is the evaporation rate, and D is the particle diffusion coefficient in the liquid droplet, which is estimated by the Einstein-Stokes relation. The Einstein-Stokes relation is expressed by $D = k_B T/6\pi\mu_l r_p$ where k_B, T, μ_l, and r_p are Boltzmann constant, temperature, liquid viscosity, and the particle radius, respectively [55]. When $Pe \ll 1$, the particles have enough time to diffuse through the droplet, which leads to

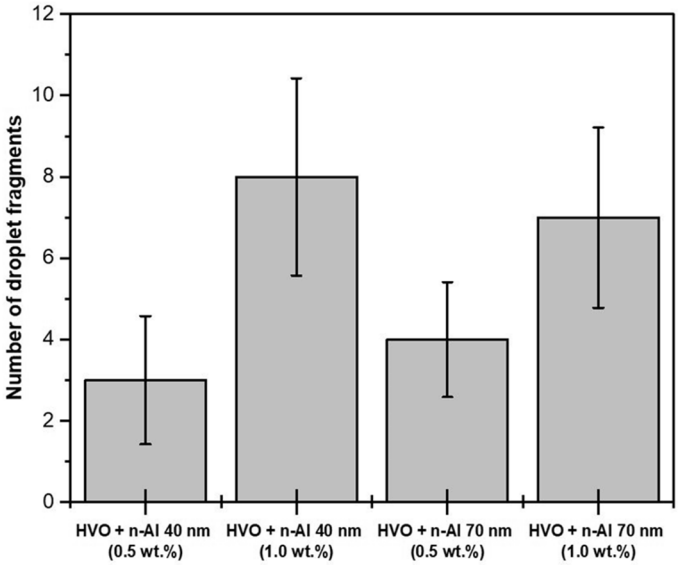

Fig. 10. Number of fragments as a quantification method for micro-explosion intensity at the end of the dry - out phase.

packed spherical particle aggregate. On the other hand, when $Pe \gg 1$, the time to diffuse the particles through the droplet is insufficient, resulting in an accumulation on the droplet surface. Consequently, taking into consideration Eq. 4 and based on the physical properties of the investigated system, an approximately value for the value of Pe was estimated to be of the order of 1000, i.e. $Pe \gg 1$. The values of r_p were 20 and 35 nm. Regarding the temperature, T was approximately 280 °C acquired from the distillation curve [47] and the viscosity values were obtained from [31,48]. This Pe value asserts that the particles are agglomerating at the droplet surface before notable particle redistribution occurs by diffusion. The liquid biofuel is evaporating more quickly than the aluminum particles diffusion, evidencing that convective transport dominates over the diffusive transport.

In the present work, the visualization of nanoparticle aggregation inside the droplet is not possible. However, through image analysis, it was detected a short period of an approximately constant droplet diameter at the end of the droplet lifetime, indicating the presence of aggregation. The disruption of the primary droplet begins at t = 38 ms. At this instant, the solid phase has a predominant role. The suppressing of the vaporization of the biofuel increases the droplet temperature. This process leads to the biofuel vapor nucleation, promoting the ejection of solid particles agglomerates. These aluminum particles ignite and promote small bright spots. However, few nanoparticles remain in the primary droplet and are continuously exposed to the high ambient temperature, leading to ignition. This event leads to aluminum combustion when no more liquid fuel persists, being identified by intensely bright spots, which gradually extinguishes at t = 43 ms. Afterward, the final combustion residue is violently projected away, ending up ascending as the smoke tail. The final residue was not collected, due to impossibility in the experimental setup. The combustion residues are expelled through the exhaust, however, the impact and influence of these products can be evaluated in more concrete conditions such as in a spray. Studies on nanofuels spray combustion are truly scarce. In this way, understanding how nanoparticles enhance biofuel performance and the effect micro-explosions and radiation in the combustion process would reinforce the potential use of nanofuels.

Fig. 9 shows a sequence of images depicting the micro-explosion of HVO + n-Al 40 nm (1.0 wt.%). Before the ejection of aluminum particles, the droplet diameter is approximately constant for a short period of time at the end of the droplet lifetime, as observed for the lowest concentration. Similar to the observations reported in the previous paragraphs, for the HVO + n-Al 40 nm (0.5 wt.%) droplets, the disruption of the primary droplet begins with the ejection of particles agglomerates leading to their ignition. As already mentioned, at the end of the droplet lifetime, the vapor nucleation of the biofuel leads to an intense micro-explosion due to the increase of the nanoparticle concentration at the droplet surface. This phenomenon can be identified at instant t = 34 ms due to the ejection and combustion of several aluminum aggregates in different directions. These disruptive burning events are dependent on particle concentration, indicating that the micro-explosions intensity increases for higher nanoparticle concentration. For all nanofuel droplets, micro-explosion is detected and its intensity varies greatly in respect to the particle concentration, being a minimal difference in the particle size. Micro-explosions for nanofuel droplets present a probability occurrence of 100 %. In virtue of these observations, micro-explosion intensity is related to the number and distribution of fragments ejected from the primary droplet in the present work.

Fig. 10 shows the average number of fragments released when the primary droplet disrupts due to the micro-explosion, for all investigated nanofuels. To evaluate the micro-explosion intensity, a simple and empirical method was employed. The number of droplet fragments is counted through image data processing, when the fragment size is larger than the pixel size. The results show that increasing the nanoparticle concentration leads to an increase in the number of fragments and an increase in the projection distance. However, for lower concentrations (0.5 wt.%), a weaker fragmentation occurs, indicating a decrease in the micro-explosion intensity. It is important to highlight that in future works, alternative techniques should be employed (e.g. acoustic and temperature sensor measurements) for validating the present method. Additionally, the nanoparticle concentration also influences micro-explosion delay. As mentioned before, when analyzing the results depicted in Fig. 6, the micro explosion delay decreases for higher nanoparticle concentrations. The micro-explosions delay is related to the accumulation of aluminum nanoparticles and to the appearance of a local hot spot inside the droplet. Increasing the particle concentration in the biofuel, the number of particles inside the droplet is higher and the solid phase becomes predominant earlier in the droplet lifetime, resulting in a decrease in micro-explosions delay when compared to nanofuels with lower particle concentration.

Regarding the particle size, a pronounced difference in the results of this investigated range suggests that it has a small effect on micro-explosion intensity when compared to particle concentration. Based on the experiments, the nanofuels combustion can be divided into five stages: preheating, ignition, combustion, micro-explosion, and

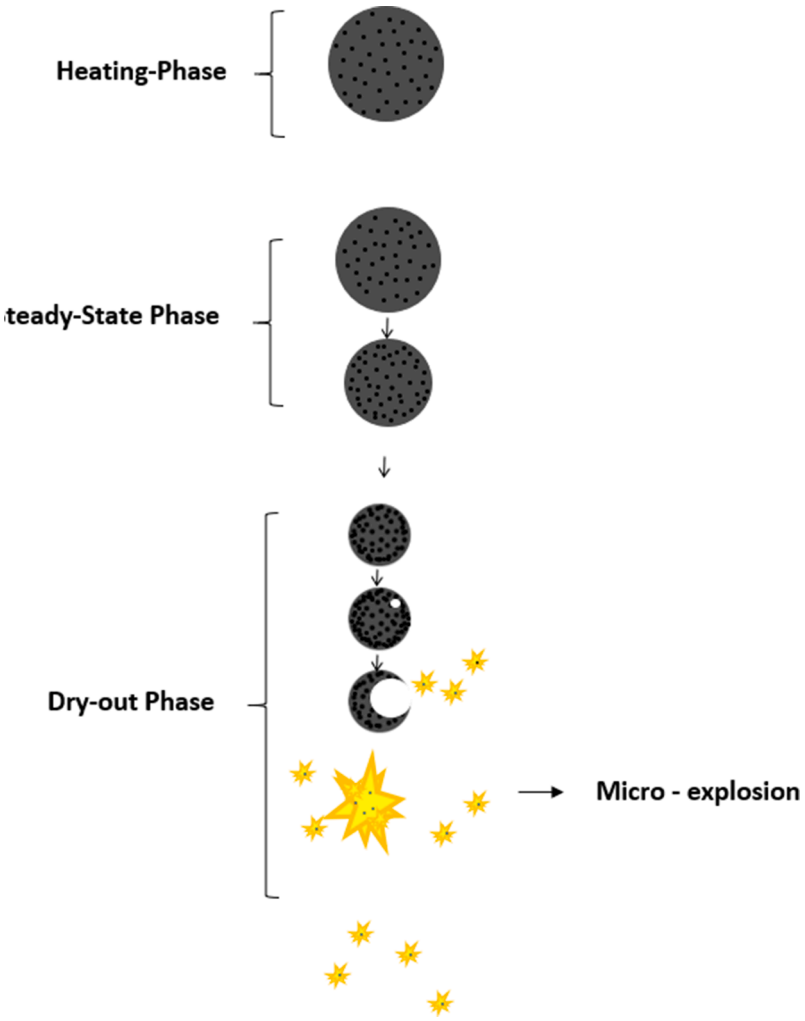

Fig. 11. Schematic diagram of single droplet combustion, including an illustration of a micro-explosion.

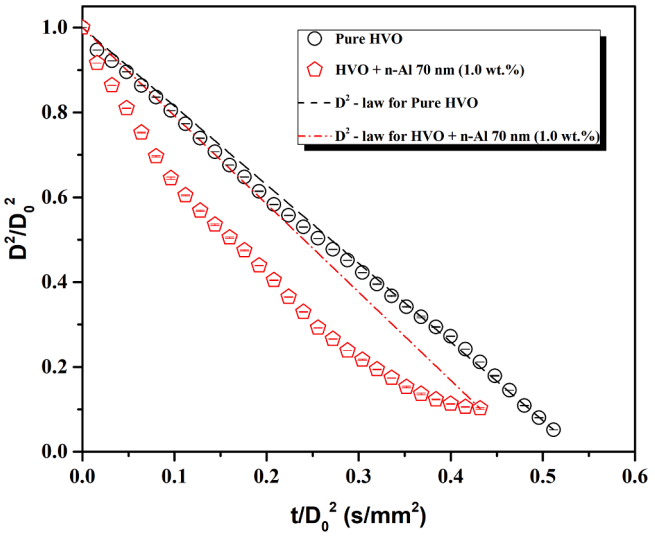

Fig. 12. Square of the normalized droplet diameter as a function of the normalized time at 1100 °C for pure HVO and HVO + n-Al 70 nm (1.0 wt.%) (D_0 = 250 μm, atmospheric pressure).

aluminum combustion. Fig. 11 shows the schematic diagram of the different phases present in the nanofuel droplet combustion, including an illustration of a micro- explosion at the dry-out phase. At the initial stage, the droplet is heated by high ambient temperature, then a reduction in its diameter is observed, as displayed at the steady - state phase. Finally, at the dry - out phase, a micro-explosion appears for all the nanofuel regardless of particle size and concentration. As mentioned, liquid fuel evaporation promotes an increase in the particle concentration inside the droplet surface. Due to the presence of these particles, the local hot spot appears, inducing the biofuel vapor nucleation and, consequently the occurrence of a micro-explosion. During this process, the particle agglomeration ignites, pronouncing the aluminum combustion. After this, the disintegration of the primary droplet reveals the end of the droplet. Despite the differences observed in intensity and in the micro-explosion delay, the appearance of micro-explosions significantly reduces the droplet lifetime for both sizes and concentrations, as will be described in detail in the following section.

3.3. Droplet size evolution and burning rate: A comparison between pure biofuel and a nanofuel

This section is dedicated to a comparison between a pure biofuel and a nanofuel to provide insights and detailed description for different evaporation phases. Fig. 12 shows the square of the normalized droplet diameter as a function of the normalized time for pure HVO and HVO + n-Al 70 nm (1.0 wt.%). The temporal evolution of the droplet size

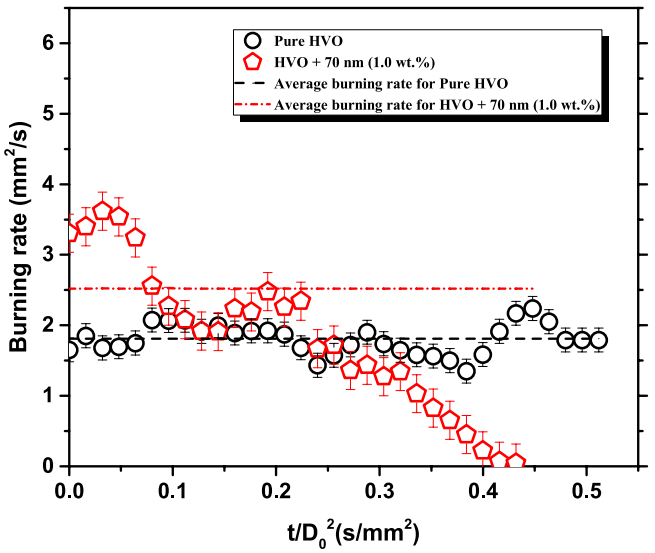

Fig. 13. Temporal evolution of burning rate and average burning rate for the pure HVO and HVO + 70 nm (1.0 wt.%) (D_0 = 250 μm, T = 1100 °C, atmospheric pressure).

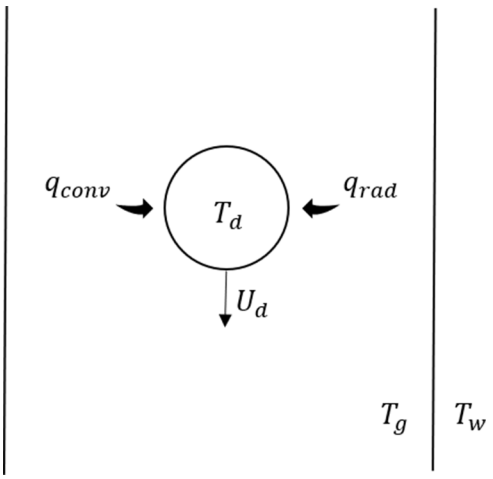

Fig. 14. Schematic diagram of a falling droplet in the drop tube furnace (T_d - Droplet temperature, T_g - Ambient temperature, T_w - Wall temperature).

reduction for the pure HVO is in good agreement with the well - known D^2 law, as shown in Fig. 12. The classical liquid droplet combustion theory states that the normalized square diameter decreases linearly with time, with a nearly constant slope, defined as the burning rate (K).

The results show that the falling droplet of pure HVO burns as a fully liquid droplet without disruptive burning phenomena. [41] evaluated the burning characteristics of HVO single droplets in a drop tube furnace. The authors observed no micro-explosions during the combustion of HVO. However, the burning rate reported by [41] is relatively smaller due to their different experimental conditions where was also considered smaller droplet diameters. Additionally, adding aluminum nanoparticles to the pure HVO affects the temporal evolution of droplet size reduction, as noticed in Fig. 6 and Fig. 7. Through the comparison of the pure HVO with the nanofuel, it can be seen that the nanofuel presents a steeper droplet size regression curve hence reaches the $(D/D_0)^2 = 0.38$ earlier than the pure biofuel. The droplet size evolution of nanofuels does not follow the D^2 law and is in agreement with the qualitative description of nanofuel droplet evaporation and combustion, as discussed in the previous paragraphs. At the later stages of the droplet lifetime, the formation of the nanoparticle aggregates evidence a reduction in evaporation, showing a different evolution of the curve. During the steady - state phase, the droplet diameter is being reduced considerably, and a few oscillations and contractions occur without pronouncing evidence in the droplet size evolution curves. Additionally, no micro-explosions are detected at this stage.

Aluminum nanoparticles aggregation at the droplet surface difficult the vaporization of liquid fuel that remains at the end of the droplet lifetime. Consequently, the normalized squared diameter of the nanofuel is approximately constant for a few instants, until a micro-explosion occurs. This disruptive burning event is fundamentally influenced by the particle concentration and determines the end of the nanofuel droplet lifetime. These phenomena were intensively studied for emulsions, composed of fuels with different boiling points, in diverse conditions, leading to micro-explosions [57]. For a nanofuel involving a liquid fuel and nanoparticles, the appearance of micro-explosions has a different explanation. In nanofuels, there are the presence two different phases (solid and liquid phase). In this respect, the occurrence of micro-explosions leads to secondary atomization, dispersing particle agglomerate and remain liquid fuel which promotes a reduction in the droplet lifetime.

For a better understanding of the curves shown in Fig. 12, the temporal evolution of burning rate and average burning rate for the pure HVO and HVO + 70 nm (1.0 wt.%), are displayed in Fig. 13. For the analysis, 40 droplets were considered.

For the pure liquid biofuel, the average burning rate is approximately 1.81 mm^2/s, represented by a horizontal dashed black line. The analysis of the instantaneous values indicates that this fuel is evaporating without abrupt variations, meaning that it is almost constant. Nevertheless, for HVO + 70 nm (1.0 wt.%), the average burning is 2.52 mm^2/s, and the presence of nanoparticles influence the droplet behavior in the evaporation process. As shown in Fig. 12, in the early stages, the temporal evolution of the burning rate is considerably higher than the average burning rate until approximately $t/D_0^2 = 0.18\ (s/mm^2)$. Then, the liquid fuel continues to be consumed, and the instantaneous values begin to decrease. As shown in Fig. 13, the steady - state phase can be divided into two stages. The first stage corresponds to a higher burning rate than that obtained for pure HVO. Then, the burning rate decreases and at some point, its values are lower than those for the pure biofuel. A plausible explanation for this evidence is reported by [14]. At the first stage, until $t/D_0^2 = 0.18\ (s/mm^2)$, the burning rate increases due to radiation absorption. After this, the temporal evolution of the burning rate decreases due to the nanoparticles aggregation that offers a resistance to evaporation.

The reduction is significantly evident at the dry-out phase, beginning approximately at $t/D_0^2 = 0.38\ (s/mm^2)$. This result is due to the increase in the solid phase/liquid phase ratio as time evolves, affecting the burning rate. The droplet size reduction leads to an increase of nanoparticles concentration within the droplet, indicating burning rate values closer to zero at the end of the nanofuel lifetime.

The end of the first stage was considered when the burning rate decreases linearly at approximately $t/D_0^2 = 0.18\ (s/mm^2)$. Fig. 13 shows that between the instants at $t/D_0^2 = 0.16\ (s/mm^2)$ and $t/D_0^2 = 0.20\ (s/mm^2)$, the burning rate values are in the vicinity of the average burning rate and then begins to decrease significantly. Regarding the last stage, $t/D_0^2 = 0.38\ (s/mm^2)$, this instant was selected due to the burning rate values closer to zero indicating the dry-out phase.

The enhancement of the burning rate in a nanofuel is also due to the addition of particles that increase the effective thermal conductivity. According to [32], the droplet temperature increases as a consequence of the radiative absorption. Thus, the droplet evaporation increases compared to the pure biofuel, regardless of the particle size and concentration.

To enhance the knowledge regarding nanofuel evaporation behavior, a simplified macroscopic model should be developed in future works to compare with the classical liquid droplet combustion theory. Fig. 14

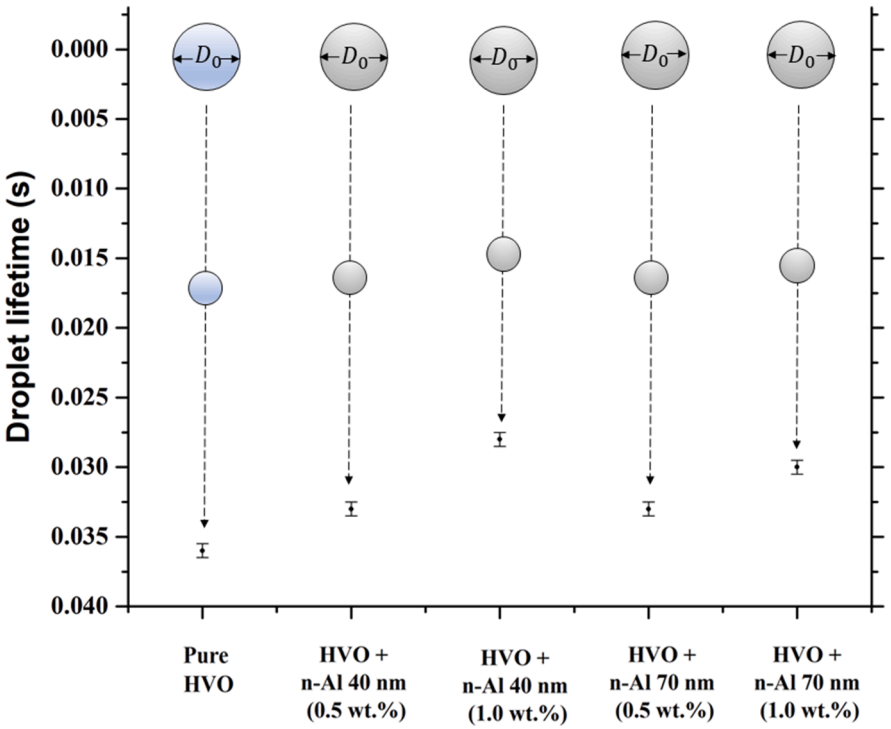

Fig. 15. Droplet lifetime for pure HVO and four nanofuels (D_0 = 250 μm, T = 1100 °C, atmospheric pressure).

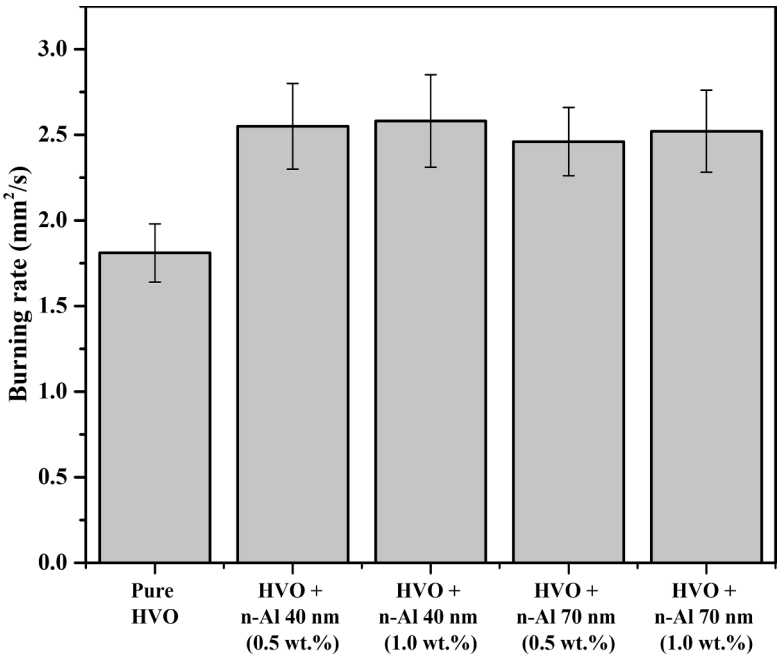

Fig. 16. Average burning rate of pure HVO and four nanofuels (D_0 = 250 μm, T = 1100 °C, atmospheric pressure).

shows a schematic diagram of a falling droplet in the drop tube furnace where heat exchanges by convection and radiation are highlighted. To evaluate the effective contribution, in particular, of radiation in nanofuels, more detailed studies should be developed relating the influence of the concentration of particles and also involving specific parameters such as wall temperature or emission/absorption coefficients [51].

The burning rate for all the fuels studied in the present work will be discussed below.

3.4. Droplet lifetime and average burning rate

Fig. 15 shows a comparison of the droplet lifetime for the fuels. At t = 0 s, the initial droplet diameter for all the fuels is 250 μm and droplet lifetime corresponds to the time of the total consumption of the primary droplet. As already mentioned, the droplet of pure HVO depicts a longer lifetime when compared with the nanofuel droplets. For the nanofuels, regardless of the size and concentration of aluminum particles, a disruptive burning phenomenon occurs, pronouncing the end of the droplet lifetime. An increase in the particle concentration leads to an

increase in the micro-explosion intensity and an earlier occurrence. Thus, droplets of HVO + n-Al 40 nm (1.0 wt.%) present an earlier micro-explosion and more intense than HVO + n-Al 40 nm (0.5 wt.%). Similar results are noticed for the nanofuels with a larger particle size (70 nm). For the investigated range of particle size, its effect is negligible on droplet lifetime. Droplets of HVO + n-Al 40 nm with the highest nanoparticle concentration have the shortest burning time for the experimental conditions studied in this work. Overall, pure HVO droplets depict the longest lifetime, while HVO + n-Al 40 nm (1.0 wt.%) has the shortest.

Droplet burning rates for pure HVO and each nanofuel are displayed in Fig. 16. The results presented in this figure were acquired not taking into account the dry - out phase $t/D_0^2 = 0.38\ (s/mm^2)$, where an approximately constant droplet diameter is observed for the nanofuels. Hence, the burning rates present in Fig. 16 do not include the end of the droplet lifetime. As mentioned earlier, 40 droplets were analyzed to evaluate the average burning rate of the fuels, which was determined by $K = -d(D^2)/dt$.

Pure HVO has a lower average burning rate than the nanofuels. This means that the addition of nanoparticles has considerable relevance in enhancing the average burning rate of biofuel. Various findings are focused on mechanisms that truly contribute to the enhancement of the burning rate which considers the radiation absorption, thermal conductivity, and micro-explosions, as already referred by [14,50,51] and mentioned in the present work.

By comparing the nanofuels, it was noticed that the higher burning rate corresponds to HVO with the smallest aluminum particles (40 nm). Regarding the particle concentration, it was observed that an increase in particle concentration promotes an increase in the burning rate. For a concentration of 1.0% of 40 nm added to HVO, the increase of the burning rate is approximately 40%. On the contrary, the particle size increase leads to a decrease of burning rates, being HVO + n-Al 70 nm (0.5 wt.%) the nanofuel with the lowest burning rate. The average burning rate is not significantly different for the various nanofuels tested here based on the measurements performed. The particle size does not vary significantly, however, it gives information regarding the influence of the nanoparticle dynamic in a liquid fuel where the primary goal was to increase biofuel performance through nanoparticles addition. Regardless of the particle size and concentration, a notable improvement in the burning of biofuel was observed. A table (Table 5) with the relative improvement due to the addition of aluminum nanoparticles can be found in appendix A.

Subsequently, further studies covering a wider range of temperatures and nanoparticle sizes should be performed in order to confirm if the nanofuel behavior is also maintained at different ambient temperatures.

4. Conclusions

The burning characteristics of pure HVO and HVO with aluminum nanoparticles were experimentally investigated in a drop tube furnace at the ambient temperature of 1100 ºC. The present work allows the study of reduced droplet diameter burned at a high ambient temperature without the use of a supporting fiber was investigated. In this respect, more realistic behavior was evaluated to highlight the effect of nanoparticles in a suitable biofuel for the aviation sector. Different sizes and concentrations of aluminum nanoparticles were added to the HVO and evaluated in terms of droplet size regression and micro-explosion. The main conclusions from this study are summarized as follows:

- The falling droplets ignited when entering the quartz tube. Subsequently, a flame was observed at the wake of the droplet for each fuel. Pure HVO droplets display a longer lifetime when compared to nanofuels. The nanofuels present a disruptive burning phenomenon at the end of the droplet lifetime.

Table 5
Relative values for burning rate and droplet lifetime.

Nanofuels	Burning rate [%]	Droplet lifetime reduction [%]
HVO + n-Al 40 nm (0.5%)	40.9	8.3
HVO + n-Al 40 nm (1.0%)	42.5	22.2
HVO + n-Al 70 nm (0.5%)	35.9	8.3
HVO + n-Al 70 nm (1.0%)	39.2	16.7

- Combustion characteristics of pure HVO can be enhanced through the addition of nanoparticles to the biofuel. This was experimentally supported in this study by observing several disruptive burning phenomena, which occur at the end of droplet lifetime. The micro-explosion intensity increases with an increase in the aluminum nanoparticles concentration. The micro-explosion delay is also influenced by particle concentration, decreasing with the increase of particle concentration.
- Droplets of HVO follow the D^2 law until the end of the droplet lifetime. However, for nanofuels, the droplet size evolution does not follow the D^2 law being evident at the dry - out phase present at the latter stage of droplet lifetime.
- The nanofuel HVO + 40 nm (1.0%) is the most promising fuel, presenting the highest burning rate and lowest droplet lifetime. In contrast, pure HVO displays the lowest burning rate.
- The effect of particle size (for the investigated range study in the present work) was not noticeable on droplet lifetime and micro-explosion intensity.

CRediT authorship contribution statement

Inês A. S. Ferrão: Methodology, Software, Data curation, Formal analysis, Investigation, Writing - original draft. **André R.R. Silva:** Conceptualization, Methodology, Validation, Resources, Writing - review & editing, Supervision, Funding acquisition. **Ana. S.O.H. Moita:** Conceptualization, Methodology, Resources, Writing - review & editing, Supervision, Funding acquisition. **Miguel A.A. Mendes:** Conceptualization, Resources, Writing - review & editing, Supervision, Funding acquisition. **Mário M.G. Costa:** Resources, Writing - review & editing, Project administration, Funding acquisition.

Declaration of Competing Interest

The authors declare that they have no known competing financial interests or personal relationships that could have appeared to influence the work reported in this paper.

Acknowledgments

The present work is dedicated to the memory of Professor Mário Costa, who participated in this project but unfortunately left us unexpectedly on 3rd June 2020. Inês Ferrão acknowledges Fundação para a Ciência e Tecnologia (FCT) for the provision of Ph.D scholarship with the reference SFRH/BD/144688/2019. The present work was performed under the scope of the Laboratório Associado em Energia, Transportes e Aeronáutica (LAETA) and Laboratório de Robótica e Sistemas de Engenharia (LARSyS) activities and it was supported by Fundação para a Ciência e Tecnologia (FCT) through the projects numbers UIDB/50022/2020 and UIDB/50009/2020. Authors would also like to acknowledge Fundação para a Ciência e Tecnologia for partially supporting this work through project JICAM/0003/2017.

Appendix A

References

[1] Asibor JO, Ighodaro O. Steady state analysis of nanofuel droplet evaporation. Int J Nanosci Nanotechnol 2019;15:145–55.
[2] Avedisian C, Andres R. Bubble nucleation in superheated liquid–liquid emulsions. J Colloid Interface Sci 1978;64:438–53.
[3] Avedisian CT, Skyllingstad K, Cavicchi RC, Lippe C, Carrier MJ. Initiation of flash boiling of multicomponent miscible mixtures with application to transportation fuels and their surrogates. Energy Fuels 2018;32:9971–81.
[4] Baranski J, Hoke J, Litke P, Schauer F. Preliminary characterization of bio-fuels using a small scale gas turbine engine, in. In: 49th AIAA Aerospace Sciences Meeting including the New Horizons Forum and Aerospace Exposition; 2011. p. 694.
[5] Basu S, Miglani A. Combustion and heat transfer characteristics of nanofluid fuel droplets: A short review. Int J Heat Mass Transf 2016;96:482–503.
[6] Bauen A, Bitossi N, German L, Harris A, Leow K. Sustainable aviation fuels. Johnson Matthey. Technol Rev 2020.
[7] Bennewitz JW, Badakhshan A, Talley DG. Combustion characteristics of suspended hydrocarbon fuel droplets with various nanoenergetic additives. Combust Sci Technol 2020:1–26.
[8] Blakey S, Rye L, Wilson CW. Aviation gas turbine alternative fuels: A review. Proc Combust Inst 2011;33:2863–85.
[9] Chiong MC, Chong CT, Ng JH, Lam SS, Tran MV, Chong WWF, Jaafar MNM, Valera-Medina A. Liquid biofuels production and emissions performance in gas turbines: A review. Energy Convers Manage 2018;173:640–58.
[10] Chishty, W.A., Davison, C.R., Bird, J., Chan, T., Cuddihy, K., McCurdy, M., Barton, P., Krasteva, A., Poitras, P., 2011. Emissions assessment of alternative aviation fuel at simulated altitudes, in: Turbo Expo: Power for Land, Sea, and Air, pp. 51–61.
[11] Clayton, R., Back, L., 1989. Physical and chemical characteristics of cenospheres from the combustion of heavy fuel oil.
[12] Dimitriadis A, Seljak T, Baškovič UŽ, Dimaratos A, Bezergianni S, Samaras Z, Katrašnik T, et al. Improving pm-nox trade-off with paraffinic fuels: A study towards diesel engine optimization with hvo. Fuel 2020;265:116921.
[13] Doliente SS, Narayan A, Tapia JFD, Samsatli NJ, Zhao Y, Samsatli S. Bio-aviation fuel: A comprehensive review and analysis of the supply chain components. Front Energy Res 2020;8:110.
[14] Emekwuru NG. Nanofuel droplet evaporation processes. J Indian Inst Sci 2019;99:43–58.
[15] Ferrão I, Vasconcelos D, Ribeiro D, Silva A, Barata J. A study of droplet deformation: The effect of crossflow velocity on jet fuel and biofuel droplets impinging onto a dry smooth surface. Fuel 2020;279:118321.
[16] Gan Y, Lim YS, Qiao L. Combustion of nanofluid fuels with the addition of boron and iron particles at dilute and dense concentrations. Combust Flame 2012;159:1732–40.
[17] Gan Y, Qiao L. Combustion characteristics of fuel droplets with addition of nano and micron-sized aluminum particles. Combust Flame 2011;158:354–68.
[18] Gan Y, Qiao L. Evaporation characteristics of fuel droplets with the addition of nanoparticles under natural and forced convections. Int J Heat Mass Transf 2011;54:4913–22.
[19] Gan Y, Qiao L. Radiation-enhanced evaporation of ethanol fuel containing suspended metal nanoparticles. Int J Heat Mass Transf 2012;55:5777–82.
[20] Gong, Y., Kaario, O., Tilli, A., Larmi, M., Tanner, F., 2010. A computational investigation of hydrotreated vegetable oil sprays using RANS and a modified version of the RNG $k-\varepsilon$ model in OpenFOAM. Technical Report. SAE Technical Paper.
[21] Guerieri PM, DeCarlo S, Eichhorn B, Connell T, Yetter RA, Tang X, Hicks Z, Bowen KH, Zachariah MR. Molecular aluminum additive for burn enhancement of hydrocarbon fuels. J Phys Chem A 2015;119:11084–93.
[22] Gür TM. Review of electrical energy storage technologies, materials and systems: challenges and prospects for large-scale grid storage. Energy Environ Sci 2018;11:2696–767.
[23] Hileman JI, Ortiz DS, Bartis JT, Wong HM, Donohoo PE, Weiss MA, Waitz IA. Near-term feasibility of alternative jet fuels. Technical Report. Rand Corporation. 2009.
[24] Hileman JI, Stratton RW, Donohoo PE. Energy content and alternative jet fuel viability. J Propul Power 2010;26:1184–96.
[25] IATA, 2018. IATA Forecast Predicts 8.2 Billion Air Travelers in 2037. Technical Report.
[26] Incropera FP, Lavine AS, Bergman TL, DeWitt DP. Fundamentals of heat and mass transfer. Wiley; 2007.
[27] Jackson G, Avedisian C. Combustion of unsupported water-in-n-heptane emulsion droplets in a convection-free environment. Int J Heat Mass Transfer 1998;41:2503–15.
[28] Javed I, Baek SW, Waheed K. Effects of dense concentrations of aluminum nanoparticles on the evaporation behavior of kerosene droplet at elevated temperatures: The phenomenon of microexplosion. Exp Thermal Fluid Sci 2014;56:33–44.
[29] Javed I, Baek SW, Waheed K, Ali G, Cho SO. Evaporation characteristics of kerosene droplets with dilute concentrations of ligand-protected aluminum nanoparticles at elevated temperatures. Combust Flame 2013;160:2955–63.
[30] Jones M, Li CH, Afjeh A, Peterson G. Experimental study of combustion characteristics of nanoscale metal and metal oxide additives in biofuel (ethanol). Nanoscale Res Lett 2011;6:1–12.
[31] Kägo R, Ilves R, Küüt A, Olt J. A review of the behavior of fuel drops in a fuel spray in the context of biofuels. J Power Technol 2019;99:218–30.
[32] Kim DM, Baek SW, Yoon J. Ignition characteristics of kerosene droplets with the addition of aluminum nanoparticles at elevated temperature and pressure. Combust Flame 2016;173:106–13.
[33] Klingshirn CD, DeWitt M, Striebich R, Anneken D, Shafer L, Corporan E, Wagner M, Brigalli D. Hydroprocessed renewable jet fuel evaluation, performance, and emissions in a t63 turbine engine. J Eng Gas Turbines Power 2012;134.
[34] Lee CC, Tran MV, Tan BT, Scribano G, Chong CT. A comprehensive review on the effects of additives on fundamental combustion characteristics and pollutant formation of biodiesel and ethanol. Fuel 2020;288:119749.
[35] Lee DS, Fahey DW, Forster PM, Newton PJ, Wit RC, Lim LL, Owen B, Sausen R. Aviation and global climate change in the 21st century. Atmos Environ 2009;43:3520–37.
[36] Li H, Rosebrock CD, Wu Y, Wriedt T, Mädler L. Single droplet combustion of precursor/solvent solutions for nanoparticle production: Optical diagnostics on single isolated burning droplets with micro-explosions. Proc Combust Inst 2019;37:1203–11.
[37] Liu JZ, Chen BH, Wu TT, Yang WJ, Zhou JH. Ignition and combustion characteristics and agglomerate evolution mechanism of aluminum in nal/jp-10 nanofluid fuel. J Therm Anal Calorim 2019;137:1369–79.
[38] Liu YC, Savas AJ, Avedisian CT. The spherically symmetric droplet burning characteristics of jet-a and biofuels derived from camelina and tallow. Fuel 2013;108:824–32.
[39] Moita AS, Laurência C, Ramos JA, Prazeres DMF, Moreira ALN. Dynamics of droplets of biological fluids on smooth superhydrophobic surfaces under electrostatic actuation. J Bionic Eng 2016;13:220–34.
[40] Nylund, N.O., Erkkilä, K., Ahtiainen, M., Murtonen, T., Saikkonen, P., Amberla, A., Aatola, H., 2011. Optimized usage of NExBTL renewable diesel fuel: OPTIBIO. Technical Report.
[41] Pacheco G, Silva A, Costa M. Single-droplet combustion of jet a-1, hydroprocessed vegetable oil, and their blends in a drop-tube furnace. Energy Fuels 2021.
[42] Patruno, A., Amicarelli, V., Lagioia, G., 2017. Aviation fuel evolution: A review.
[43] Pizziol B, Costa M, Panão MO, Silva A. Multiple impinging jet air-assisted atomization. Exp Thermal Fluid Sci 2018;96:303–10.
[44] Rochelle D, Najafi H. A review of the effect of biodiesel on gas turbine emissions and performance. Renew Sustain Energy Rev 2019;105:129–37.
[45] Sazhin S, Rybdylova O, Crua C, Heikal M, Ismael M, Nissar Z, Aziz ARB. A simple model for puffing/micro-explosions in water-fuel emulsion droplets. Int J Heat Mass Transf 2019;131:815–21.
[46] Sim HS, Plascencia MA, Vargas A, Bennewitz JW, Smith OI, Karagozian AR. Effects of inert and energetic nanoparticles on burning liquid ethanol droplets. Combust Sci Technol 2018;191:1079–100.
[47] Šimáček P, Souček I, Pospíšil M, Vrtiška D, Kittel H. Impact of hydrotreated vegetable oil and biodiesel on properties in blends with mineral diesel fuel. Thermal Sci 2019:315.
[48] Sirviö, K., Niemi, S., Heikkilä, S., Hiltunen, E., et al., 2018. Kinematic viscosity studies for medium-speed ci engine fuel blends.
[49] Tanvir S, Biswas S, Qiao L. Evaporation characteristics of ethanol droplets containing graphite nanoparticles under infrared radiation. Int J Heat Mass Transf 2017;114:541–9.
[50] Tanvir S, Qiao L. Effect of addition of energetic nanoparticles on droplet-burning rate of liquid fuels. J Propul Power 2015;31:408–15.
[51] Tanvir S, Qiao L. Droplet burning rate enhancement of ethanol with the addition of graphite nanoparticles: Influence of radiation absorption. Combust Flame 2016;166:34–44.
[52] Tyagi H, Phelan PE, Prasher R, Peck R, Lee T, Pacheco JR, Arentzen P. Increased hot-plate ignition probability for nanoparticle-laden diesel fuel. Nano Letters 2008;8:1410–6.
[53] Wang J, Huang X, Qiao X, Ju D, Sun C. Experimental study on effect of support fiber on fuel droplet vaporization at high temperatures. Fuel 2020;268:117407.
[54] Wang R, Pan G, Qian S, Li L, Zhu Z. Influence of nanoparticles on the evaporation behavior of nanofluid droplets: A dh law and underlying mechanism. Langmuir 2019;36:919–30.
[55] Wei Y, Deng W, Chen RH. Effects of insoluble nano-particles on nanofluid droplet evaporation. Int J Heat Mass Transf 2016;97:725–34.
[56] Xiu-Tian-Feng E, Pan L, Wang F, Wang L, Zhang X, Zou JJ. Al-nanoparticle-containing nanofluid fuel: synthesis, stability, properties, and propulsion performance. Ind Eng Chem Res 2016;55:2738–45.
[57] Yang J, Jackson G, Avedisian C. Combustion of unsupported methanol/dodecanol mixture droplets at low gravity, in. In: Symposium (International) on Combustion. Elsevier; 1991. p. 1619–25.
[58] Yaws CL. Chemical properties handbook. McGraw-Hill Education; 1999.
[59] Zhang H, Fang Y, Wang M, Appels L, Deng Y. Prospects and perspectives foster enhanced research on bio-aviation fuels. J. Environ. Manage. 2020;274:111214.